PCCP

PAPER

View Article Online
View Journal | View Issue

Cite this: *Phys. Chem. Chem. Phys.*, 2024, **26**, 3020

Electron transfer reaction of TEMPO-based organic radical batteries in different solvent environments: comparing quantum and classical approaches†

Souvik Mitra, [a] Andreas Heuer [ab] and Diddo Diddens [*b]

Received 25th August 2023,
Accepted 14th December 2023

DOI: 10.1039/d3cp04111e

rsc.li/pccp

In this study, we delve into the complex electron transfer reactions associated with the redox-active (2,2,6,6-tetramethylpiperidin-1-yl)oxyl (TEMPO), a common component in organic radical batteries (ORBs). Our approach estimates quantum electron-transfer (ET) energies using Density Functional Theory (DFT) calculations by sampling from structures simulated classically. This work presents a comparative study of reorganization energies in ET reactions across different solvents. Furthermore, we investigate how changes in the electrolyte environment can modify the reorganization energy and, consequently, impact ET dynamics. We also explore the relationship between classical and quantum vertical energies using linear regression models. Importantly, this comparison between quantum and classical vertical energies underscores the role of quantum effects, like charge delocalization, in offering added stabilization post-redox reactions. These effects are not adequately represented by the classical vertical energy distribution. Our study shows that, although we find a significant correlation between the vertical energies computed by DFT and the classical force field, the regression parameters depend on the solvent, highlighting that classical methods should be benchmarked by DFT before applying them to novel electrolyte materials.

Introduction

Emerging research in the field of energy storage has been highlighting the pivotal role of organic radical batteries (ORBs)[1,2] due to their potential for high power density and fast charge/discharge rates. Uniquely, these ORBs present a promising alternative to conventional lithium-ion batteries, given their cost-effective and environmentally friendly aspects, derived primarily from the use of abundant and non-toxic organic materials. Among various organic radicals, 2,2,6,6-tetramethylpiperidin-1-oxyl (TEMPO) stands out due to its promising role as a redox-active group in polymer electrodes for ORBs,[3] showcasing unique electron transfer (ET) mechanisms characterized by diffusive charge transport behavior. In this context, Marcus theory,[4,5] a widely employed method for understanding the dynamics of ET reactions in redox systems, is often utilized.

Within the semi-classical framework of Marcus theory,[5,6] electron transfer reactions are described in terms of the polarization of the solvent induced by the charges carried by the donor and acceptor solute (in complex solvent systems, other effects such as charge transfer and hydrogen bonding can facilitate electron transfer). According to this theory, the solvation effect is represented by two intersecting free energy surfaces, known as diabatic states, which correspond to the reactant and product states involved in the ET process. The occurrence of electron transfer is facilitated by the presence of significant thermal fluctuations, allowing the system, initially situated near the minimum of one diabatic state, to reach the transition state denoted by the point at which the reactant and product states intersect, where electron can tunnel from the initial diabatic state to the final diabatic state, with the probability governed by the Landau–Zener formula.[7] Subsequent to the electron hopping event, the system experiences a relaxation phase characterized by the reorientation of surrounding solvent molecules and the structural optimization of the solute entities. The energy associated with this intricate process is defined as the reorganization energy, a fundamental factor in the dynamics of ET reactions within these redox systems.

In the original conception of Marcus theory,[6] polarization was represented as the linear response of a dielectric continuum. As a result, the impact of the solvent could be encapsulated in a singular parameter. Apart from the assumption of

[a] *Institute of Physical Chemistry, University of Münster, Corrensstraße 28/30, 48149 Münster, Germany*
[b] *Helmholtz-Institute Münster (IEK-12), Forschungszentrum Jülich GmbH, Corrensstraße 46, 48149 Münster, Germany. E-mail: d.diddens@fz-juelich.de*

† Electronic supplementary information (ESI) available. See DOI: https://doi.org/10.1039/d3cp04111e

linear response not only legitimizes the quadratic dependency of free energy surfaces on the reaction coordinate, Marcus theory also postulates identical curvatures for the resulting parabolas of the two free energy surfaces. A microscopic characterization of the polarization order parameter was notably introduced by Warshel *et al.*,[8] who incorporated the vertical energy gap as a reaction coordinate for ET reactions. This vertical energy gap serves as a quantitative indicator of the electron's energy preference for the donor site over the acceptor site, offering greater insight into the mechanisms of ET reactions. Their work is of significant importance as the choice of vertical energy gap as reaction coordinate in their study reveals that, under the linear response assumption, the reorganization energy of ET reactions is inversely proportional to the curvature of the resulting free energy parabolas.

The quantum mechanically calculated vertical energy gap encompasses the electron's delocalization in the donor orbital and the subsequent electronic relaxation following ET phenomena, which are not accounted for by the classically calculated vertical energy. The change in the shape of the free energy profiles, when utilizing the quantum vertical energy gap as a reaction coordinate, compared to the classical solvent electrostatic potential, was demonstrated by Blumberger *et al.*[9] in their study on aqueous Ru^{2+} solutions using density functional theory (DFT) based molecular dynamics (MD) simulations. In their study, it was shown that in the absence of this orbital delocalization information, the classical vertical energy gap leads to a reduced curvature in the free energy parabola and consequently an increase in reorganization energy compared to its quantum counterpart.

Both *ab initio* MD (AIMD)[10] and hybrid quantum/classical (QM/MM)[11] approaches, although capturing quantum effects, are constrained by relatively short time trajectories on the order of a few picoseconds. The time trajectories in these systems can be significantly shorter than (1) the average time between two ETs and (2) the typical relaxation time of the local molecular environment, the latter of which leads to insufficient statistical sampling. Moreover, challenges are often posed in accurately predicting smooth distributions due to the scarcity of structures derived from these short time trajectories. In contrast, classical MD[12] simulations, while potentially lacking certain quantum mechanical information, offer the advantage of encompassing significantly longer trajectories. By employing reliable force fields, a wider range of structural variations can be explored, and well-defined free energy profiles can be generated.

As part of this work, to calculate quantum vertical energy, density functional theory (DFT) calculations were performed on a small subset of the structures generated using classical MD simulation. In this way, we guarantee sufficient sampling of local solvation environments, while still obtaining additional information about the orbital energies of the transferred electron or about electronic polarization effects. Oxidation of TEMPO radical (TEMPO.) and reduction of TEMPO cation ($TEMPO^+$) in water[13] were considered to verify our method.

The second part of this work explored how changes in the electrolyte environment can impact the reorganization energies of ET reactions. In our study, the commonly employed electrolyte ethyl carbonate(EC)/ethyl methyl carbonate(EMC)/$LiPF_6$, recently also utilized in ORBs,[2,14–18] was chosen to investigate the influence of the electrolyte environment on the ET reaction dynamics. With regard to battery applications, we observe a significant impact of the electrolyte composition on the reorganization energy and hence, the estimated electron hopping rate. Notably, these findings suggest that it is important to adjust the solvent composition in order to optimize the electron hopping rate.

Finally, we will attempt to establish a relation between classical and quantum ET distributions using linear regression models. Furthermore, we explore the possibility of calculating ET reorganization energies directly through classical simulations. Although the quantum and classical energies are strongly linearly correlated for a given solvent, the predictive power of classical simulations appears to be limited.

Theory and methods

Marcus theory

Marcus introduced intersecting diabatic free energy surfaces for the reactant state (R) and the product state (P) to describe a homogeneous ET reaction.[6] In his study, Marcus employed the semi-classical approximation to separate the ET rate into two components: the electronic coupling parameter and the Franck–Condon factor.[9,19,20] The Franck–Condon factor, representing the probability of nuclear reorganization in the ET process, can be studied independently of the electronic coupling. This assumption in Marcus theory allows for the decomposition of the overall diabatic states for a homogeneous ET reaction into the energy surfaces of the oxidation (ox) and reduction (red) processes separately.

These free energy surfaces, denoted as A_M (where M refers to ox or red), are assumed to have a quadratic behavior with respect to a reaction coordinate denoted as x:

$$A_M(x) = A_M^0 + \frac{k_M}{2}(x - x_M)^2, \quad M = \text{ox, red} \qquad (1)$$

Here, x_{ox} and x_{red} represent the equilibrium values of the reaction coordinate in the reactant and product states, respectively. A_M^0 and k_M denote the equilibrium free energy and spring constant for the energy surface M, respectively.

The reorganization free energy, a central concept in Marcus theory, is derived from the free energy profiles. Although in the original work, λ was defined for the overall forward and backward ET reactions, for a homogeneous ET reaction it can be defined separately for the oxidation and reduction states as follows:

$$\lambda_{ox} = A_{ox}(x_{red}) - A_{ox}(x_{ox}) \qquad (2a)$$

$$\lambda_{red} = A_{red}(x_{ox}) - A_{red}(x_{red}) \qquad (2b)$$

Here, λ_{ox} and λ_{red} refer to the reorganization energy for the oxidation and reduction processes, respectively.

To describe ET reactions, it is necessary to establish an appropriate reaction coordinate as the reorganization energy, λ_M, relies on the choice of a suitable reaction coordinate. In their work, Warshel *et al.*[8] incorporated the complete microscopic configuration of the system, denoted as R^N (*i.e.*, the coordinates of all N atoms in the system), into x by selecting the vertical energy ($\Delta E(R^N)$). For oxidation and reduction processes, the vertical energies are given by:

$$\Delta E_{ox}(R^N) = E_{ox}(R^N) - E_{red}(R^N) \quad (3a)$$

$$\Delta E_{red}(R^N) = E_{red}(R^N) - E_{ox}(R^N) \quad (3b)$$

Here, $E_M(R^N)$ and $\Delta E_M(R^N)$ represent the diabatic potential energy and vertical energy for the state M, respectively, where M = ox, red. The diabatic free energy function A_M takes the form:

$$A_M(\Delta E_M) = -k_B T \ln P_M(\Delta E_M) + \text{const} \quad (4a)$$

$$P_M(\Delta E_M) = \langle \delta_{\Delta E_M} \rangle_M \quad (4b)$$

In the above equations, P_M represents the probability distribution of ΔE, δ is the Dirac delta function, and the brackets $\langle \cdots \rangle_M$ denote the Boltzmann or ensemble averages over the diabatic space M (in our work, $\langle \cdots \rangle_M$ was determined from the time average instead, because the system was assumed to be ergodic[21]).

Based on the definition, the diabatic free energies for the same structure, as they correspond to no change in entropy, satisfy the following relationship:

$$A_{ox}(\Delta E) - A_{red}(\Delta E) = \Delta E_{ox} \quad (5a)$$

$$A_{red}(\Delta E) - A_{ox}(\Delta E) = \Delta E_{red} \quad (5b)$$

By selecting ΔE as the coordinate, eqn (2a) and (2b) can be rewritten as:

$$\lambda_{ox} = A_{ox}(\Delta E_{red}^{min}) - A_{ox}(\Delta E_{ox}^{min}) \quad (6a)$$

$$\lambda_{red} = A_{red}(\Delta E_{ox}^{min}) - A_{red}(\Delta E_{red}^{min}) \quad (6b)$$

Here, ΔE_M^{min} refers to the energy minimum of the diabatic state M.

Under the quadratic approximation of the free energy with respect to ΔE_M as the coordinate, the probability distribution $P_M(\Delta E_M)$ can be assumed to follow a Gaussian distribution:

$$P_M(\Delta E) = \frac{1}{\sigma_M \sqrt{2\pi}} e^{-\frac{1}{2}\left(\frac{\Delta E - \langle \Delta E \rangle_M}{\sigma_M}\right)^2} \quad (7)$$

Here, σ_M denotes the standard deviation of the distribution. Manipulating the properties of diabatic free energy states (eqn (5a), (5b), (6a), (6b)) in combination with the quadratic approximation (eqn (1)), the relation between λ_M and the spring constant k_M can be expressed as:

$$\lambda_M = \frac{1}{2 \times k_M} \quad (8)$$

Now, as k_M can be derived from the second derivative of the free energy parabola, which can be obtained from eqn (7) and (4a), it gives a relationship with σ_M:

$$k_M = \frac{k_B T}{\sigma_M^2} \quad (9)$$

From eqn (9) and (8), we can derive the following relationship:

$$\lambda_M = \frac{\sigma_M^2}{2 k_B T} \quad (10)$$

The relationship given in eqn (10) will play a pivotal role in this study. This equation would also serve as operational definition of lambda even if the distributions are not fully Gaussian.

MD simulations

To validate our proposed method, oxidation of TEMPO. and reduction of $TEMPO^+$ were considered. To implement this, two distinct simulations were conducted, one with TEMPO. and another with $TEMPO^+$. Each simulation involved 66 water molecules, allowing for a comprehensive assessment of our method's performance on both species.

Classical MD simulations were performed using GROMACS 2019.[22] To obtain a DFT-compatible box size for future quantum calculations, a small simulation cell was considered for MD simulations. The initial configurations in a 1.7 × 1.7 × 1.7 nm^3 simulation cell, were constructed using PACKMOL,[23] which avoids repulsive potentials by keeping a safe inter-atomic distance. Periodic boundaries in all three Cartesian coordinates were considered. Prior to the equilibration run, a short initial MD run was performed to obtain a dense system as well as removing any unrealistic or high-energy configurations that may have arisen during the initialization of the system, for 2 ns with a 0.5 fs time step. To efficiently densify the system, the pressure was set to 100 bar for this relaxation step, ensuring a more compact and stable arrangement of the molecular components. In this relaxation step, both temperature and pressure were controlled with a Berendsen thermostat and a Berendsen barostat,[12,24] respectively, both with time constants of 1.0 ps. The reference temperature was taken as 298.15 K. The Coulombic interactions were handled using a particle–particle particle–mesh (PPPM) solver with a cutoff of 0.6 nm, which was also applied to the Lennard-Jones interactions. This short cutoff was compatible with the NPT simulation performed in such a small simulation box. Following the relaxation step, dense systems with dimensions of approximately 1.3 nm were obtained. For the equilibration step, NVT simulations for both oxidation and reduction processes were performed for 20 ns with 1 fs time step with the dense systems obtained after the relaxation step. In this case, temperature were controlled with a Nosé–Hoover thermostat with time constants of 1.0 ps. The rest of the parameters were the same as the relaxation step. Finally for the collection of data, a 100 ns simulation with the exact same parameters as used for the equilibration step was run for each of the two systems.

The OPLS all-atom force field[25] was used for all the MD simulations. The atomic site charges on both TEMPO radical and cation were calculated from the electrostatic potential

(ESP) fit (Fig. S1, ESI†). Gaussian16[26] was used to calculate the ESP charges using MP2 theory[27] with pVDZ basis set.[28]

For the second part of our work, the same simulation setup was replicated by replacing water with 10 EC molecules and 5 EMC molecules to recreate the electrolyte environment. Additionally, simulations were conducted by introducing 1 $LiPF_6$ salt ion pair to the system. These variations in the simulation setup allowed us to investigate the influence of different electrolyte components on the system's behavior and further validate our method.

Vertical energy calculations

From the equilibrium trajectory of the Classical MD simulation of TEMPO. ($TEMPO^+$) in water, 50 000 frames were taken at intervals of 2 ps. From each frame, potential energies were calculated both before and after altering the TEMPO radical (cation) to its corresponding cation (radical) form without changing the atomic coordinates. The classical vertical energies were then determined by computing the energy difference between these two states.

For the calculation of quantum vertical energies, a subset of 195 frames was selected from the 50 000-frame trajectory. The selection of these 195 structures was made at intervals of 400 ps. For each of these 195 MD frames, single point energies were computed using the DFT method in Vienna *ab initio* simulation package (VASP),[29] which is based on the plane wave pseudo-potential method. Core states were treated with the Projected Augmented Wave (PAW) technique.[30] For the exchange–correlation (XC) functional, the generalized gradient approximation (GGA) was employed, specifically adopting the Perdew–Burke–Ernzerhof (PBE) parametrization.[31] The cutoff energy for the plane waves was set to 520 eV. For Brillouin zone integration, a Γ-centered $1 \times 1 \times 1$ Monkhorst–Pack grid and Gaussian smearing with a width of 0.01 eV were employed. The threshold for the self-consistency criterion in solving the Kohn–Sham equations was set at 10^{-5} eV.

All the input files for the quantum calculation in VASP are available in Zenodo.[32]

The quantum vertical energies were derived from the energy difference between these two states. To assess the impact of the DFT functionals[33,34] on the vertical energies, we performed comparison calculations for 3 randomly chosen structures (shown in ESI,† Table S1). These calculations show that the choice of the functional has a marginal influence on the vertical energies. Note that for both the classical and quantum energies, the presence of a net TEMPO charge results in self-interactions, and there may be differences due to the various implementations in Gromacs and VASP. However, since our main interest lies in determining the reorganization energy (λ) from the width of the vertical energy distribution (σ), any potential shift due to these technical factors should be similar across all frames, making it an uncritical factor in our analysis.

Similar calculations were performed to calculate the classical and quantum vertical energies for TEMPO in EC/EMC and EC/EMC/$LiPF_6$ mixture. In these systems, classical vertical energies were calculated for 50 000 structures, while quantum vertical energies were calculated for 95 structures.

Linear regression model

In order to establish the relationship between the quantum results and their classical counterpart, linear regression analysis was performed:

$$Y_i^Q = aX_i^C + b + \varepsilon_i \quad (11)$$

Here, Y_i^Q is the quantum vertical energy for the ith frame and X_i^C is its classical counterpart (here, "Q" and "C" stand for quantum and classical, respectively). b and a are intercept and slope of the linear fit, respectively. ε_i is the random error term accounted for the variation between the observed quantum result, Y_i, and its predicted value obtained from the linear fit. This analysis aimed to determine the correlation and

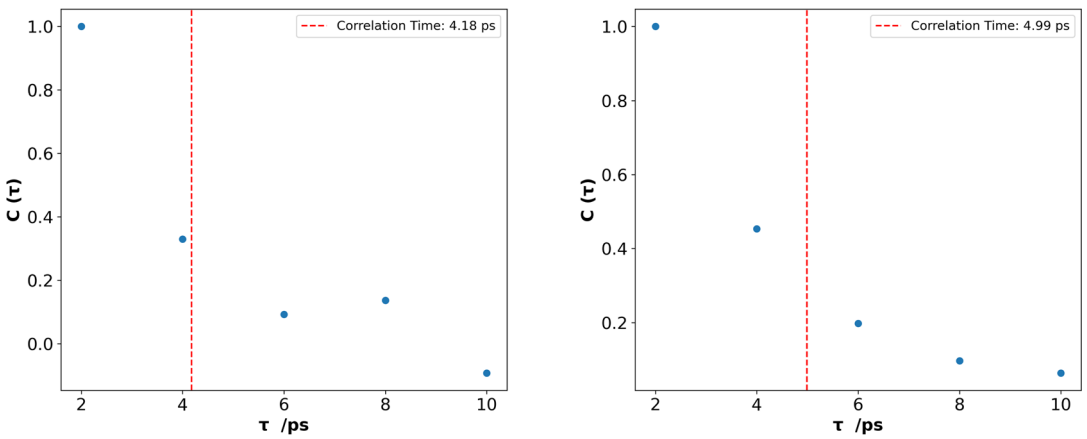

(a) Vertical energy correlation for oxidation of TEMPO·. (b) Vertical energy correlation for reduction of $TEMPO^+$.

Fig. 1 Vertical energy correlation, $C(\tau) = \frac{\langle \Delta E(0) \cdot \Delta E(\tau) \rangle - \langle \Delta E \rangle^2}{\langle \Delta E^2 \rangle}$ for (a) oxidation of TEMPO. and (b) reduction of $TEMPO^+$ in water. Correlation times are shown by the red dotted lines.

quantify the degree of agreement between the quantum and classical data sets.

Results and discussion

Quantum vertical energy distribution for TEMPO in water

The vertical energy correlation time was found to be 4 to 5 ps for both oxidation of TEMPO. and reduction of $TEMPO^+$ in water (Fig. 1). Here, correlation time is calculated (using exponential fitting: $\exp\left(-\frac{\tau}{\tau_0}\right)$, where τ and τ_0 are time and correlation time, respectively) as the time at which the correlation function drops to $1/e$. This implies that it takes this amount of time to obtain statistically uncorrelated structures. Consequently, unlike classical MD, methods such as AIMD, or hybrid QM/MM methods cannot produce a large number of statistically uncorrelated structures and as a result calculating a clear vertical energy distribution is not possible with such methods. This motivated the sampling of configurations by classical MD, followed by single-point DFT calculations as described in the Methods section.

Distributions that are approximately Gaussian were observed for quantum vertical energies calculated from 195 statistically uncorrelated structures (see Fig. 2a and b). From the direct calculation of the second moment, σ^Q_M and eqn (10), λ^Q_M were found to be 0.63 eV and 0.7 eV for M = ox and M = red, respectively, at a temperature of 298.15 K.

The deviation in λ^Q for the oxidation and reduction processes can be attributed to the different charge states of the solute and the varying orientations of the surrounding solvent molecules.

Below, we present a table comparing the values of λ^Q_M for both the oxidation of TEMPO and the reduction of $TEMPO^+$ across three different solvents.

In the next section, we will discuss the quantum vertical energies obtained for the oxidation of TEMPO. and the reduction of $TEMPO^+$ in EC/EMC mixture both in the presence and absence of salt $LiPF_6$.

Impact of electrolyte environment on ET characteristics

As mentioned in the introduction, carbonate electrolytes, usually applied in commercial lithium ion batteries, have recently also been employed in ORBs,[2,14–18] which are promising as next-generation energy storages. Therefore, in this section, quantum vertical energy distributions for TEMPO dissolved in carbonate mixtures, both with and without lithium salt, were calculated. For each of these cases, 95 statistically uncorrelated structures were chosen.

In Table 1, while all λ^Q_M values fall within the same range, we note a deviation in λ^Q_{ox} and λ^Q_{red} for non-aqueous solvents similar to the aqueous case, presumably due to slight differences in the solvation shells of TEMPO and $TEMPO^+$.

Interestingly, the oxidation process of TEMPO. in the presence of EC and EMC solvents revealed a significant increase in σ^Q_{ox}, leading to a corresponding increase in λ^Q_{ox}, when a single $LiPF_6$ was added to the binary solvent (see Fig. S2a and c, ESI†). In particular, a 40% increase in λ^Q_{ox} was observed when going from the binary EC/EMC mixture to the EC/EMC/$LiPF_6$ electrolyte (Table 1).

Similar to the oxidation process, reduction processes of $TEMPO^+$ to its radical in the presence of EC and EMC solvents, showed a significant increase in σ^Q_{red} when a single $LiPF_6$ was added (see Fig. S2b and d, ESI†). A 32% increase in λ^Q_{red} was observed when going from the binary EC/EMC mixture to the EC/EMC/$LiPF_6$ electrolyte (Table 1).

In the presence of salt, an increase in reorganization energy for both the oxidation and reduction processes occurs, as Li^+ prefers coordination with solvent molecules, resulting in increased rigidity[35,36] of the solvent and making it less likely to reorient during the charge transfer reaction. This coordination is justified by the radial distribution function (RDF) plots included in the ESI† (see Fig. S11 and S12).

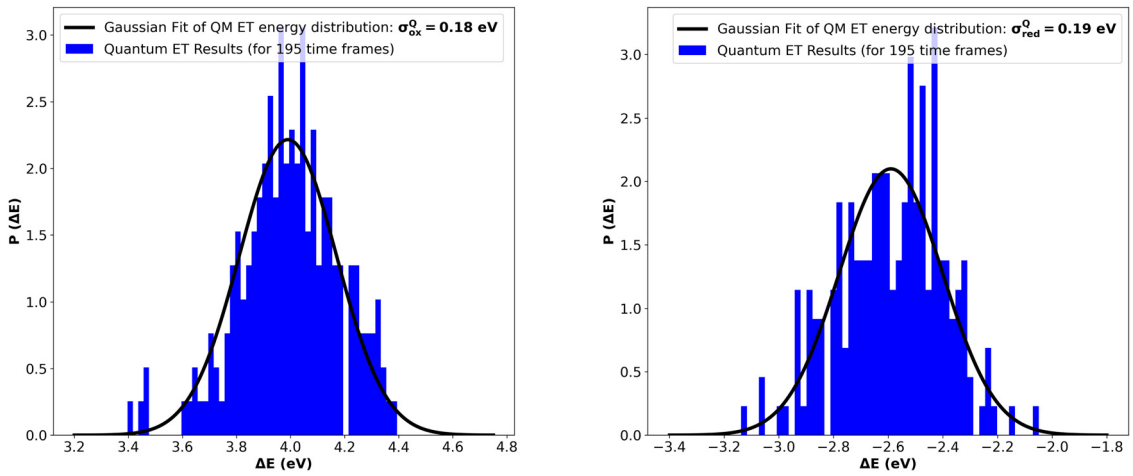

(a) Oxidation of TEMPO · (b) Reduction of $TEMPO^+$

Fig. 2 Quantum vertical energy distribution (a) for the oxidation of TEMPO. in water and (b) for the reduction of $TEMPO^+$ in water.

Table 1 Comparison of λ_M^O for the oxidation of TEMPO as well as the reduction of $TEMPO^+$ in three different solvents at a temperature of 298.15 K

Solvent	Redox step	λ_M^O (eV)
Water	Oxidation	0.63
	Reduction	0.7
EC/EMC mixture	Oxidation	0.5
	Reduction	0.77
EC/EMC/$LiPF_6$ mixture	Oxidation	0.7
	Reduction	1.02

Experimental calculations of reorganization energies in aqueous[13] and non-aqueous solvents[37] have been found to yield values similar to those observed in our study. Experiments indicate that reorganization energy plays a crucial role in charge hopping in organic electrodes,[15,16,38] and it has also been observed that the composition of the electrolyte can heavily influence the reorganization energy.[14,37]

In the framework of Marcus theory,[6] the activation energy (E_a) for electron transfer between a donor and an acceptor is determined by the reorganization energy, as expressed by the equation $E_a = \frac{(\Delta G^0 + \lambda)^2}{4\lambda}$. Here, ΔG^0 and λ represent the standard Gibbs free energy change and the reorganization energy for the reaction, respectively. Considering the case of charge transfer events between a TEMPO radical and a TEMPO cation, where ΔG^0 can be considered as zero, it is observed that the activation energy increases with an increase in λ. Consequently, this relationship implies that charge transfer events of this nature in the system are inversely related to the reorganization energy. Our study reveals that the addition of salt leads to an increase in reorganization energy, thereby suggesting a decrease in charge transfer events between a TEMPO radical and a TEMPO cation.

In total, our results demonstrate that the reorganization energy may strongly depend on the local environment. Specifically, it demonstrates that the addition of ions increases the reorganization energy for both the oxidation and reduction processes by providing additional stability to the redox center. This will especially be the case for multicomponent systems employed in ORBs.[2] Therefore, these considerations will be important for the directed optimization of ORB cathode materials. Tuning the electrolyte composition can also optimize electron transfer dynamics in the organic radical electrode. For instance, it's plausible that various types of salts influence the stability trends of both the oxidised and neutral states of redox centers, subsequently impacting the dynamics of the ET reaction.

Correlation between quantum and classical vertical energies

Having observed that the electrolyte environment is crucial to describe the vertical energy distribution, one might wonder in how far these effects are already contained in the classical force field employed in the MD simulations. To elucidate this, we first determined the correlation between quantum and classical vertical energies for the oxidation of TEMPO. and reduction of $TEMPO^+$ for different solvents from their scatter plots (see Fig. 3 and Fig. S6, ESI†). Moderate but significant correlations are expressed by correlation coefficients in the range from 0.5 to 0.7.

In the ESI,† we show that not only the vertical energies (*i.e.* energy difference between both diabatic states) of the classical and the quantum mechanical model are correlated, but also the individual diabatic energies (see Fig. S3 and S4, ESI†). Moreover, when fitting a straight line to the data, we note that the residuals of both diabatic states are correlated as well (Fig. S3c and S4c, ESI†).

We derived a statistical relation (eqn (S8), ESI†) to relate the correlation of classical and quantum vertical energies to the underlying correlation of the residuals of both diabatic states. Remarkably, although the correlation in Fig. 3 appears rather moderate, it can only be achieved when the correlation of residuals for both diabatic states is extremely good, with correlation coefficients of about 0.93.

Therefore, one might be tempted that quantum vertical energies can be predicted solely from the classical vertical

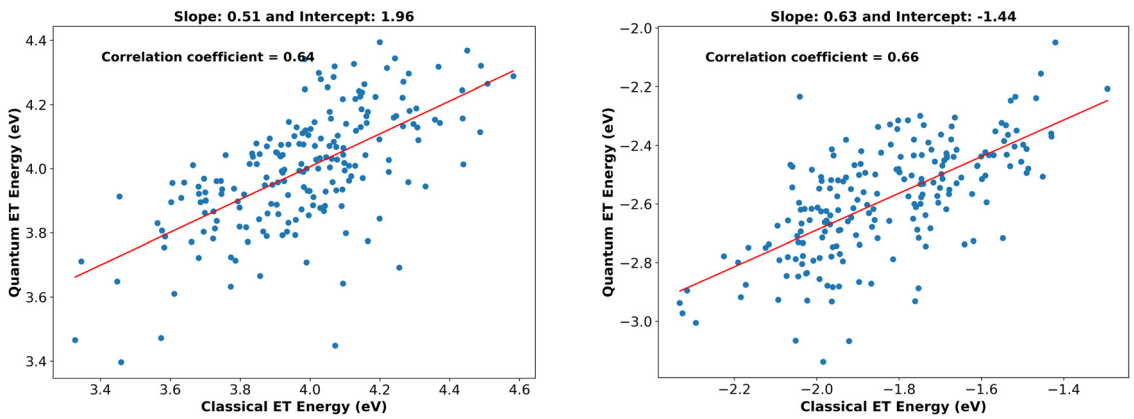

(a) Oxidation of TEMPO · (b) Reduction of $TEMPO^+$

Fig. 3 Scatter plots between classical and quantum vertical energies for (a) oxidation of TEMPO. and (b) reduction of $TEMPO^+$ in water.

Table 2 Comparison of σ_M^Q, a_M, σ_M^C and σ_M^ϵ for the oxidation of TEMPO as well as the reduction of $TEMPO^+$ in three different solvents

Solvent	Redox step	σ_M^Q (eV)	a_M	σ_M^C (eV)	σ_M^ϵ (eV)
Water	Oxidation	0.18	0.51	0.22	0.14
	Reduction	0.19	0.63	0.2	0.14
EC/EMC mixture	Oxidation	0.16	0.54	0.2	0.12
	Reduction	0.2	0.61	0.24	0.13
EC/EMC/$LiPF_6$ mixture	Oxidation	0.19	0.42	0.26	0.16
	Reduction	0.23	0.69	0.24	0.16

energies without conducting any quantum calculations. However, as we will demonstrate in the subsequent section, this is not the case.

Establishing relation between σ^C and σ^Q from Linear regression

As observed in Fig. 3 and Fig. S6 (ESI†), the relation between classical and quantum vertical energies can be reasonably well described by a linear relation (eqn (11)). Similarly, from the standard deviation (σ_M^C) of classical vertical energies and the standard deviation (σ_M^ϵ) of the error term, standard deviation (σ_M^Q) of Quantum vertical energies of state M (here, M = ox, red), relevant for the calculation of λ_M^Q, can be predicted based on eqn (11), which follows:

$$\sigma_M^{Q^2} = {a_M}^2 \times \sigma_M^{C^2} + \sigma_M^{\epsilon^2} \quad (12)$$

In this equation, a_M and σ_M^ϵ represent the slope and standard deviation of the error term from the scatter plot of quantum and classical vertical energies, respectively (see Fig. 3 and Fig. S6, ESI†).

Below, we present a table comparing the values of σ_M^Q, a_M, σ_M^C and σ_M^ϵ for both the oxidation of TEMPO and the reduction of $TEMPO^+$ across three different solvents.

From Table 2, it becomes evident that both a_M and σ_M^ϵ are not constant values, indicating that they are dependent on the system under consideration (naively one might assume that solely σ_M^C depends on the system). Hence, one cannot generally predict σ_M^Q only from σ_M^C without performing any quantum calculations.

If the classically obtained standard deviation σ_M^C were identical to the quantum value σ_M^Q, classical simulations would offer a highly efficient alternative to quantum calculations. However, as seen from Table 2, this is not the case. Classical simulations might still have predictive power for the impact of the solvent if σ_M^C and σ_M^Q were directly correlated when comparing results across different solvents. Unfortunately, Fig. 4 shows that, in the case of reduction reactions, the data are not correlated. This suggests that the apparent correlation observed in oxidation reactions may merely be a result of the small sample size. The absence of this correlation is directly tied to the significant variation in the slope a_M for different solvents.

These variations in values may at least partly arise from the variation in polarization effects induced by the presence of different solvents. In this context, it's worth noting that our OPLS all-atom force field[25] does not account for the polarization effect. Therefore, using a polarizable force field[39] might result in uniform a_M and σ_M^ϵ.

Another interesting observation of our study is that we noticed a lower value of σ_M^Q compared to σ_M^C (Fig. 4). This decrease in σ_M^Q (and consequently in λ_M^Q) when compared to its classical counterpart aligns with the idea that charge delocalization due to quantum effects offers additional stabilization of the post-redox reaction state.[9] This induced stabilization cannot be accounted for in the classical vertical energy distribution, as it does not consider charge delocalization or electronic polarization.

Conclusions

In this work, we studied the reorganization energies of TEMPO radicals *via* sampling the vertical energies by both classical MD simulations and DFT calculations. In conclusion, from our work it has been observed that the vertical energy correlation

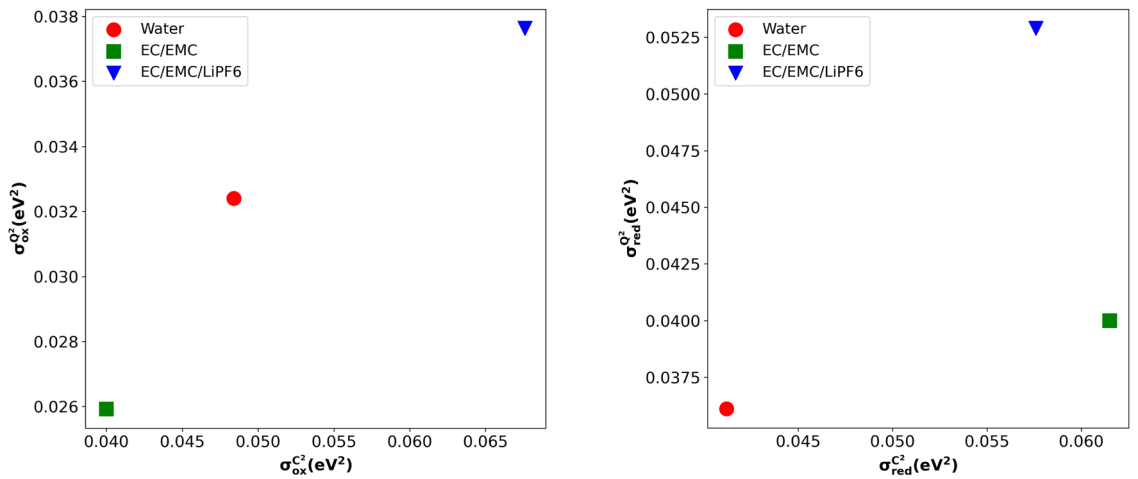

(a) Oxidation of TEMPO · (b) Reduction of $TEMPO^+$

Fig. 4 (a) $\sigma_{ox}^{Q^2}$ *vs.* $\sigma_{ox}^{C^2}$ and (b) $\sigma_{red}^{Q^2}$ *vs.* $\sigma_{red}^{C^2}$ plots for TEMPO in water (red), EC/EMC (green), and EC/EMC/$LiPF_6$ (blue).

time is around 4–5 picoseconds. This suggests that generating a large dataset of uncorrelated structures using AIMD[10] or hybrid QM/MM[11] methods is challenging for such systems. Additionally, our research has provided insights into how the electrolyte environment influences the reorganization energy and consequently impacts ET dynamics. In particular, our study demonstrates that the addition of salt increases the reorganization energy, as the increased rigidity of the solvent reduces its likelihood of reorientation during the charge transfer reaction.

Our statistical analysis shows that the quantum and classical vertical energies exhibit a good correlation, but this correlation is system-dependent. As a result, one cannot predict σ_M^Q solely from σ_M^C. The inclusion of the polarization effect into the classical force field[39] might make this prediction feasible. Nevertheless, classical MD simulations can be utilized to efficiently sample structures, which then can be subjected to quantum calculations.

A crucial observation from our study is the decrease in the quantum reorganization energy, λ_M^Q, compared to its classical counterpart, λ_M^C. This observation aligns with the theory[9] that charge delocalization, which is a quantum effect, provides additional stabilization after redox reactions.

This research has advanced our understanding of reorganization energies on single TEMPO molecules, thereby paving the way to predict local reorganization energies within an organic electrode filled with multiple redox centers. This understanding is a significant stride towards unraveling the complex ET mechanisms inside ORBs.

Conflicts of interest

There are no conflicts of interest to declare.

Acknowledgements

SM, AH and DD acknowledge funding by Deutsche Forschungsgemeinschaft [Priority Program SPP 2248 ''Polymer-based Batteries'' (project number 441255373)]. I am also grateful to Sukanya Majumdar for her continuous support.

References

1 K. Nakahara, K. Oyaizu and H. Nishide, Organic Radical Battery Approaching Practical Use, *Chem. Lett.*, 2011, **40**, 222–227.
2 D. T. Daniel, S. Oevermann, S. Mitra, K. Rudolf, A. Heuer, R.-A. Eichel, M. Winter, D. Diddens, G. Brunklaus and J. Granwehr, Multimodal investigation of electronic transport in PTMA and its impact on organic radical battery performance, *Sci. Rep.*, 2023, **13**, 10934.
3 L. Wylie, T. Blesch, R. Freeman, K. Hatakeyama-Sato, K. Oyaizu, M. Yoshizawa-Fujita and E. I. Izgorodina, Reversible Reduction of the TEMPO Radical: One Step Closer to an All-Organic Redox Flow Battery, *ACS Sustainable Chem. Eng.*, 2020, **8**, 17988–17996.
4 J. Blumberger, Recent Advances in the Theory and Molecular Simulation of Biological Electron Transfer Reactions, *Chem. Rev.*, 2015, **115**, 11191–11238.
5 R. A. Marcus, Electron Transfer Reactions in Chemistry: Theory and Experiment (Nobel Lecture), *Angew. Chem., Int. Ed. Engl.*, 1993, **32**, 1111–1121.
6 R. A. Marcus, On the Theory of Oxidation-Reduction Reactions Involving Electron Transfer. II. Applications to Data on the Rates of Isotopic Exchange Reactions, *J. Chem. Phys.*, 2004, **26**, 867–871.
7 C. Zener and R. H. Fowler, Non-adiabatic crossing of energy levels, *Proc. R. Soc. London, Ser. A*, 1932, **137**, 696–702.
8 J. K. Hwang and A. Warshel, Microscopic examination of free-energy relationships for electron transfer in polar solvents, *J. Am. Chem. Soc.*, 1987, **109**, 715–720.
9 J. Blumberger and M. Sprik, Quantum versus classical electron transfer energy as reaction coordinate for the aqueous Ru^{2+}/Ru^{3+} redox reaction, *Theor. Chem. Acc.*, 2006, **115**, 113–126.
10 J. Blumberger and M. Sprik, Ab Initio Molecular Dynamics Simulation of the Aqueous Ru^{2+}/Ru^{3+} Redox Reaction: The Marcus Perspective, *J. Phys. Chem. B*, 2005, **109**, 6793–6804, PMID: 16851765.
11 M. I. G. Nicholson, P. R. Bueno and G. T. Feliciano, Ab Initio QM/MM Simulation of Ferrocene Homogeneous Electron-Transfer Reaction, *J. Phys. Chem. A*, 2021, **125**, 25–33, PMID: 33382268.
12 D. Rapaport, *The Art of Molecular Dynamics Simulation*, Cambridge University Press, 2004.
13 H. O. Finklea and N. Madhiri, Reorganization energies of TEMPO/TEMPO+ in water, *J. Electroanal. Chem.*, 2008, **621**, 129–133, Special Issue in Honor of Professor Israel Rubinstein.
14 S. Wang, F. Li, A. D. Easley and J. L. Lutkenhaus, Real-time insight into the doping mechanism of redox-active organic radical polymers, *Nat. Mater.*, 2019, **18**, 69–75.
15 S. Iwasa, T. Nishi and S. Nakamura, Enhancement of rapid charging capability of organic radical battery using ethylene carbonate-based electrolyte containing LiFSI, *J. Power Sources*, 2018, **402**, 157–162.
16 K. Nakahara, K. Oyaizu and H. Nishide, Electrolyte anion-assisted charge transportation in poly(oxoammonium cation/nitroxyl radical) redox gels, *J. Mater. Chem. A*, 2012, **22**, 13669–13673.
17 T. W. Kemper, T. Gennett and R. E. Larsen, Molecular Dynamics Simulation Study of Solvent and State of Charge Effects on Solid-Phase Structure and Counterion Binding in a Nitroxide Radical Containing Polymer Energy Storage Material, *J. Phys. Chem. C*, 2016, **120**, 25639–25646.
18 K. Nakahara, J. Iriyama, S. Iwasa, M. Suguro, M. Satoh and E. J. Cairns, Cell properties for modified PTMA cathodes of organic radical batteries, *J. Power Sources*, 2007, **165**, 398–402.
19 K. Ando, Quantum energy gap law of outer-sphere electron transfer reactions: a molecular dynamics study on aqueous solution, *J. Chem. Phys.*, 1997, **106**, 116–126.

20 K. Ando, Solvent nuclear quantum effects in electron transfer reactions. III. Metal ions in water. Solute size and ligand effects, *J. Chem. Phys.*, 2001, **114**, 9470–9477.
21 D. McQuarrie, *Statistical Thermodynamics*, University Science Books, 1973.
22 M. Abraham, *et al. GROMACS 2023 Manual*. 2023.
23 L. Martınez, R. Andrade, E. G. Birgin and J. M. Martınez, PACKMOL: a package for building initial configurations for molecular dynamics simulations, *J. Comput. Chem.*, 2009, **30**, 2157–2164.
24 H. J. C. Berendsen, J. P. M. Postma, W. F. van Gunsteren, A. DiNola and J. R. Haak, Molecular dynamics with coupling to an external bath, *J. Chem. Phys.*, 1984, **81**, 3684–3690.
25 W. L. Jorgensen, D. S. Maxwell and J. Tirado-Rives, Development and Testing of the OPLS All-Atom Force Field on Conformational Energetics and Properties of Organic Liquids, *J. Am. Chem. Soc.*, 1996, **118**, 11225–11236.
26 M. J. Frisch *et al. Gaussian-16 Revision C.01*, Gaussian Inc., Wallingford CT, 2016.
27 P. Atkins and R. Friedman, *Molecular Quantum Mechanics*, OUP, Oxford, 2011.
28 J. Dunning and H. Thom, Gaussian basis sets for use in correlated molecular calculations. I. The atoms boron through neon and hydrogen, *J. Chem. Phys.*, 1989, **90**, 1007–1023.
29 G. Kresse and J. Furthmuller, Efficient iterative schemes for ab initio total-energy calculations using a plane-wave basis set, *Phys. Rev. B: Condens. Matter Mater. Phys.*, 1996, **54**, 11169–11186.
30 P. E. Blochl, Projector augmented-wave method, *Phys. Rev. B: Condens. Matter Mater. Phys.*, 1994, **50**, 17953–17979.
31 J. P. Perdew, K. Burke and M. Ernzerhof, Generalized Gradient Approximation Made Simple, *Phys. Rev. Lett.*, 1996, **77**, 3865–3868.
32 S. Mitra, All input files for quantum calculations in VASP, 2023, DOI: **10.5281/zenodo.8252154**.
33 A. P. Bartok and J. R. Yates, Regularized SCAN functional, *J. Chem. Phys.*, 2019, **150**, 161101.
34 S. Grimme, J. Antony, S. Ehrlich and H. Krieg, A consistent and accurate ab initio parametrization of density functional dispersion correction (DFT-D) for the 94 elements H-Pu, *J. Chem. Phys.*, 2010, **132**, 154104.
35 M. Li, J. Owrutsky, M. Sarisky, J. P. Culver, A. Yodh and R. M. Hochstrasser, Vibrational and rotational relaxation times of solvated molecular ions, *J. Chem. Phys.*, 1993, **98**, 5499–5507.
36 M. T. Ong, O. Verners, E. W. Draeger, A. C. T. van Duin, V. Lordi and J. E. Pask, Lithium Ion Solvation and Diffusion in Bulk Organic Electrolytes from First-Principles and Classical Reactive Molecular Dynamics. The, *J. Phys. Chem. B*, 2015, **119**, 1535–1545, PMID: 25523643.
37 C. Karlsson, T. Suga and H. Nishide, Quantifying TEMPO Redox Polymer Charge Transport toward the Organic Radical Battery, *ACS Appl. Mater. Interfaces*, 2017, **9**, 10692–10698, PMID: 28282111.
38 K. Zhang, Y. Xie, B. B. Noble, M. J. Monteiro, J. L. Lutkenhaus, K. Oyaizu and Z. Jia, Unravelling kinetic and mass transport effects on two-electron storage in radical polymer batteries, *J. Mater. Chem. A*, 2021, **9**, 13071–13079.
39 D. Bedrov, J.-P. Piquemal, O. Borodin, A. D. J. MacKerell, B. Roux and C. Schroder, Molecular Dynamics Simulations of Ionic Liquids and Electrolytes Using Polarizable Force Fields, *Chem. Rev.*, 2019, **119**, 7940–7995, PMID: 31141351.

